Appearance of de Sitter black holes and strong cosmic censorship

Li-Ming Cao,[1,2,*] Long-Yue Li,[2,†] Xia-Yuan Liu,[2,‡] and Yu-Sen Zhou[2,§]

[1]*Peng Huanwu Center for Fundamental Theory, Hefei, Anhui 230026, China*
[2]*Interdisciplinary Center for Theoretical Study and Department of Modern Physics, University of Science and Technology of China, Hefei, Anhui 230026, China*

(Received 3 February 2024; accepted 1 March 2024; published 10 April 2024)

We study the optical appearance of Schwarzschild–de Sitter and Reissner–Nordström–de Sitter black holes viewed by distant observers inside cosmological horizons. Unlike their asymptotically flat counterparts, due to the positive cosmological constant, there are outermost stable circular orbits in the spacetimes, resulting in significant outer edges in the images. Besides this, when the Reissner–Nordström–de Sitter black hole has a stable Cauchy horizon, the photons from the preceding companion universe can be received by the observer in our universe. These rays create a multiring structure in the image. Since the stable Cauchy horizon violates the strong cosmic censorship conjecture, this novel image sheds some light on the test of the conjecture by astronomical observations.

DOI: 10.1103/PhysRevD.109.084021

I. INTRODUCTION

Despite its incredible success, general relativity (GR) indicates its own breakdown at singularities. This was demonstrated by Hawking and Penrose [1,2], who showed that within the framework of GR, gravitational collapse inevitably leads to singularities. These singularities mark the catastrophic edge where determinism breaks down in our current understanding of physics. To remedy this issue, two conjectures were proposed: the weak cosmic censorship conjecture (WCCC) [3], and the strong cosmic censorship conjecture (SCCC) [4]. The WCCC primarily concerns the visibility of singularities by faraway observers, postulating that singularities are always concealed behind a horizon. For instance, a Kerr-Newman (KN) black hole cannot be overcharged or overspun to become a naked KN singularity by absorbing matter [5,6]. On the other hand, the SCCC is devoted to rescuing the determinism of GR. It states that a physical spacetime is always globally hyperbolic [4,7,8]. However, the extension of spacetime beyond the Cauchy horizon processed in a Reissner-Nordström (RN) black hole seems to violate the SCCC. Fortunately, the Cauchy horizon of a RN black hole has been shown to be unstable [9–15]. Several methods have been proposed to examine the validity of the SCCC within a given spacetime. For example, the perturbation of a RN black hole grows unbounded near the Cauchy horizon [9–12], and the method used involves the backreaction by considering ingoing null flux [13]. Furthermore, Poisson and Israel [14] found that the mass inflation—i.e., the divergence of the Hawking mass or renormalized Hawking mass—can be triggered by the presence of an outgoing null flux. Therefore, the Cauchy horizon of a RN black hole will convert into a null singularity after a small perturbation, which prevents the observer from passing through it. There are numerous black holes whose Penrose diagrams resemble those of the RN black hole, i.e., all diagrams consist of repeated universes. This apparent similarity appears to violate the SCCC. Fortunately, the Cauchy horizons associated with these black holes are also unstable, therefore preventing the extension beyond Cauchy horizon [16–19].

It was commonly believed that the SCCC holds true and may only be violated in some peculiar modified gravity, or when extraordinary matter is present. However, even in the context of GR, which is the most well-established theory of gravity, counter-examples exist. One such counter-example is the RN–de Sitter (dS) black hole, which is distinguished by a single additional parameter compared to the RN black hole. It is one of the most typical solutions with a nonvanishing cosmological constant. Under certain parameters, the RN-dS black hole can exhibit a stable Cauchy horizon [20–24]. Consequently, the Penrose diagram of the RN-dS black hole can be extended to consist of countless repeated, identical universes. Therefore, observers could travel through a black-white hole bridge and then enter another separate universe, which violates the SCCC. More precisely, the Cauchy horizon remains stable when the surface gravity of the Cauchy horizon is less than that of the cosmological horizon [25,26]. The mass inflation in the more sophisticated Einstein–Maxwell–scalar field model

*caolm@ustc.edu.cn
†lily26@mail.ustc.edu.cn
‡liuxiayuan@mail.ustc.edu.cn
§zhou_ys@mail.ustc.edu.cn

has been thoroughly studied in the trilogy [27–30]; in particular, a detailed range of parameters for mass inflation has been achieved.

It is widely believed in astronomy that massive stars will eventually collapse to form rotating black holes—i.e., Kerr black holes. There are many similarities between RN and Kerr black holes. For example, they both have singularities and Cauchy horizons. The Penrose diagram of the equatorial plane of a Kerr black hole is similar to that of a RN black hole. This implies that the global structure of a Kerr black hole is similar to that of a RN one to some extent. Just as the cosmological constant stabilizes the Cauchy horizon of the RN black hole, similar scenarios occur for the Kerr black hole. In other words, the Cauchy horizon of the Kerr black hole is also unstable, which respects the SCCC [31]. However, when the cosmological constant is taken into account, the Cauchy horizon of the Kerr-dS black hole can be stable for certain parameters, which violates the SCCC [32]. On the other hand, a positive cosmological constant can describe the inflation of the early universe and plays a crucial role in explaining the universe's accelerating expansion. Multiple observations now also favor a positive cosmological constant. Therefore, the Kerr-dS black hole has garnered considerable interest. In short, the similarities mentioned above even appear when they are immersed in de Sitter space. Based on the similarities, the study of the SCCC in RN-dS black holes has reference significance for the study of Kerr-dS black holes and could potentially serve as a natural experimental site for testing the SCCC.

Several years ago, images of the supermassive objects at the centers of the M87 [33] and Milky Way galaxies [34] were captured by the Event Horizon Telescope (EHT). This provides us a novel method to detect compact objects and black holes. In these black hole pictures, a bright ring surrounds a dark shadow, formed by light emitted directly from the accretion disk. According to calculations for the null geodesics, light rays emitted from the vicinity of the photon sphere, where the effective potential reaches its maximum, can circulate around the black hole numerous times before being received by the observer. A more general definition of the photon sphere (surface) can be found in [35]. However, the anticipated type of light remained undetected on these images. Utilizing a ray-tracing method [36], we can trace light rays backwards from the observer's image plane. The trajectory of light rays intersects with the accretion disk, subsequently converging to a bright ring in the image plane. Such a ring is called a "lensed ring" for the case of two intersections, and a "photon ring" for more intersections. However, the Lyapunov exponent being positive indicates that the photon sphere is chaotic. This means that the separation between two initially close trajectories will diverge exponentially over time. Consequently, the photon ring is so close to the lensed ring that they cannot be distinguished, and because it is much narrower, its contribution to the overall intensity is negligible. Lensed rings are also covered by the directly emitted light due to the current limitations of astronomical observation precision. As the impact parameter reaches its critical limit, the rays rotate at the photon sphere for infinite time. Since the accretion disk is distributed in a limited range, the rays emitted from the edge of the source will form a sharp edge on the image. The position of a lensed ring or photon ring reveals information about the background geometry, while the total appearance of a compact object is heavily influenced by the position and profile of the light source.

Recently, the images of many compact objects were studied using the ray-tracing method proposed in [36], such as Kazakov-Solodukhin black holes, regular black holes with de Sitter cores, quantum-corrected black holes, wormholes, and so on [37–44]. All of these works have exhibited the reliability of this way to get the optical appearance of black holes or other compact objects. Therefore, it is valuable to apply the method to study images of black holes when the SCCC is destroyed, and find some specific and indicative features which might provide some enlightenment on the astronomical observations. Actually, in [45], we have studied the image of a regular black hole with a stable Cauchy horizon, which is inconsistent with SCCC. The rays from the preceding companion universe can be received by the observer in our universe due to the stable Cauchy horizon. This produces many new rings inside the shadow area in the image. This novel multiring structure may be detected astronomically. The fly in the ointment is that a precise physical process that leads to the formation of such a black hole still remains a mystery. On the other hand, it is clear that the RN-dS black hole with a stable Cauchy horizon has a reasonable explanation in the framework of Einstein gravity theory. It is natural to exploit its image in the same way. However, unlike the asymptotically flat black holes, some difficulties arise when the positive cosmological constant is presented. First, for the RN-dS black hole, the observers have to be located inside the cosmological horizon rather than the null infinity. But the image is influenced greatly by the location of the observer, while there is no specific location given privileged status. The image has an outer edge if the observer is close to the black hole, and the image formed by the rays emitted directly is more narrow compared with that of a Schwarzschild black hole. Second, unlike the case of asymptotically flat black holes, there are outermost stable circular orbits (OSCOs) in the spacetime of the dS or charged dS black hole [46–48]. A physically reasonable thin accretion disk is distributed between the innermost stable circular orbit (ISCO) and the OSCO, and this leads to a significant outer edge in the image. Third, during the propagation of light, the redshift or blueshift factor in the RN-dS black hole is quite different from that in the asymptotically flat case—for example, it tends to infinity near the cosmological horizon. A very large intensity of light will be received by the observers near the

cosmological horizon. All of these phenomena will be discussed in detail in Sec. III.

As with a regular black hole with a stable Cauchy horizon, the stable Cauchy horizon in the RN-dS black hole also gives rise to the multiring structure. Hence, it may offer a potential method to test the SCCC in astronomical observations. However, the multiring structure also occurs in compact objects without horizons and in wormholes [49–52]. Furthermore, a similar multi-image structure can be found in the images of stars created by the gravitational lensing of a massive object [53,54]. The difference between these objects and a black hole violating the SCCC is whether they have horizons. In [55], a general relativistic formalism is proposed to get the parameters of the RN black hole (such as the mass and the charge) from some directly observable quantities (such as the total frequency shift, aperture angle of the telescope, and redshift rapidity). A method to get the parameter of the Kerr-dS black hole is proposed in [56]. Maybe we can distinguish between compact objects, wormholes, and the RN-dS black hole with the assistance of multiple methods, especially the experiment involving a significant redshift in the presence of an event horizon.

This paper is organized as follows: In Sec. II, we introduce the ISCO and OSCO of the RN-dS black hole and get the range when there is a stable Cauchy horizon, an ISCO and OSCO in RN-dS spacetime. In Sec. III, we draw up the image of the Schwarzschild-dS black hole and analyze the effect of observer distance on the image. Then, the image of the RN-dS black hole is investigated in Sec. IV. Finally, we give conclusions and discussions in Sec. V.

II. THE ISCO AND OSCO IN THE RN-DS BLACK HOLE

The existence of an ISCO for massive particles in the Schwarzschild black hole at $r = 6m$ is a well-known fact. However, in addition to the ISCO, there is an OSCO in the spacetime of the Schwarzschild-dS black hole or, more generally, the RN-dS black hole. Physically acceptable substances that can emit light are generally massive. As a result, we adapt the model of the accretion disk, which is regarded as the source of light emission, to consist of the stable orbits of these massive substances. Consequently, the accretion disk in a RN-dS black hole resembles a band distributed between the ISCO and OSCO. The accretion disk for a Kerr-dS spacetime is studied in [57]. In this section, we will give a brief introduction to the ISCO and OSCO of the RN-dS black hole.

In static coordinates, the metric of a RN-dS black hole can be written as

$$ds^2 = -f(r)dt^2 + \frac{1}{f(r)}dr^2 + r^2d\theta^2 + r^2\sin^2\theta d\phi^2, \quad (2.1)$$

where

$$f(r) = 1 - \frac{2M}{r} + \frac{Q^2}{r^2} - \frac{\Lambda}{3}r^2. \quad (2.2)$$

Here, M is the mass parameter, Q is the electric charge parameter, and $\Lambda > 0$ is the cosmological constant. We are interested in a case with three horizons—i.e., the Cauchy horizon, the event horizon, and the cosmological horizon. The radii of these horizons are denoted as r_-, r_+, and r_c, respectively, which are three real roots of $f(r) = 0$. With the help of the Killing vector fields $\partial/\partial t$ and $\partial/\partial\phi$, we can get the conserved quantities associated with the geodesic, which can be used to simplify the equations of motion of the particle. The motion of a particle with energy E and angular momentum l is governed by the equation

$$\dot{r}^2 + V(r) = E^2, \quad (2.3)$$

where

$$V(r) = \left(\frac{l^2}{r^2} + \epsilon\right)f(r) \quad (2.4)$$

is the effective potential. Here, $\epsilon = 0, 1$ for massless and massive particles, respectively, and an overdot denotes a derivative with respect to the parameter of the geodesic. Of course, this parameter is the so-called affine parameter when the particle is massless.

For the circular orbits, we have $V_r = 0$, where V_r denotes the derivative of V with respect to r. Similarly, in the following discussion, V_{rr} and V_{rrr} represent the second and third derivatives of V with respect to r, respectively. Furthermore, $V_{rr} < 0$ for the unstable circular orbits, and $V_{rr} > 0$ for the stable circular orbits. Solving $V_r = 0$ for the massless particles, we can get a stable photon sphere between the event horizon and the Cauchy horizon, and an unstable photon sphere outside the event horizon. However, in the case of massive particles, the situation is complicated. Figure 1 represents the parameter space of circular orbits, where each point corresponds to a unique circular orbit.[1] The curves depicted in the figure are composed of points that satisfy $V_r = 0$, representing the physically allowed circular orbits. The curves consist of two parts. The lower part, appearing almost horizontal, is concealed behind the event horizon, and thus is not of interest to us. However, the stability of a point on the curve requires further calculations on V_{rr}. As the radius r approaches positive infinity or 0, the derivative of effective potential V_r tends toward negative infinity. The V_r within the region between the two branches of the curve is positive. Intuitively, consider an auxiliary vertical line with

[1]Here and below, unless otherwise stated, all numerical values of Q, r, and l represent quantities in units of M. Similarly, Λ is given in units of M^{-2}.

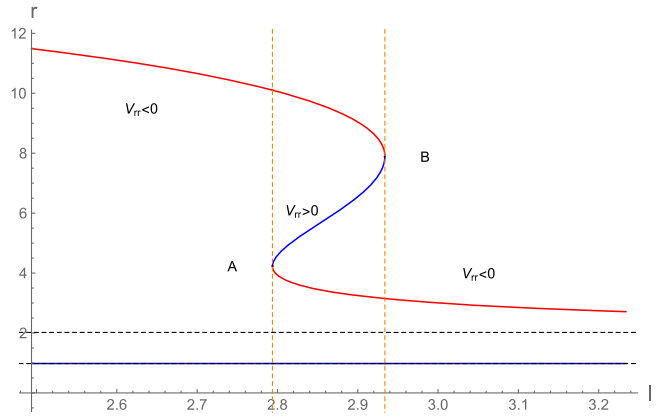

FIG. 1. The r-l diagram of a RN-dS black hole with $Q = 0.995$, $\Lambda = 0.001$. l is the angular momentum of a massive particle, and r is the corresponding circular orbital radius. The two horizontal black dashed lines are photon spheres, while the two solid curves in the figure are derived from $V_r = 0$. The lower one (blue), which is inside the event horizon, nearly overlaps with the black dashed line. The upper curve is divided into three parts by the points A and B. The segment AB (in blue) represents stable circular orbits because $V_{rr} > 0$, while the red curves represent unstable circular orbits because $V_{rr} < 0$. Therefore, A is the ISCO and B is the OSCO. The two orange vertical dashed lines, whose abscissas are l_A and l_B, represent the angular momentum l for the points A and B.

fixed l. The intersections of the line with the curve represent the zeros of V_r. As we gradually increase the value of r from bottom to top, crossing the intersections of the line and the curve, if V_r transits from negative to positive, then $V_{rr} \geq 0$. Conversely, if V_r transits from positive to negative, then $V_{rr} \leq 0$. A more rigorous discussion appears in the following paragraphs.

We have two special circular orbits represented by the points A and B where $\mathrm{d}l/\mathrm{d}r = 0$. Actually, the circular orbit associated with A where $\mathrm{d}^2l/\mathrm{d}r^2 > 0$ is simply the ISCO. Accordingly, the orbit presented by the point B where $\mathrm{d}^2l/\mathrm{d}r^2 < 0$ is the OSCO mentioned in the previous section. It should be noted that although neither point A nor point B represents a stable circular orbit since $V_r = V_{rr} = 0$, $V_{rrr} \neq 0$ at these points, stable orbits can indeed be found within any small vicinity around them. We will prove this in the next paragraph. Besides the situation depicted in Figs. 1 and 2(a), there is a critical case where the ISCO and OSCO coincide, which has been shown in Fig. 2(b). It can be seen that $\mathrm{d}^2l/\mathrm{d}r^2$ vanishes at the black spot in Fig. 2(b). Unlike the usual Schwarzschild black hole, for some range of parameters, RN-dS spacetime does not possess stable circular orbits outside the event horizon, which can be understood from Fig. 2(c). Obviously, as $l \to \infty$, the effective potential V of the massive particles tends toward that of the massless particles. Meanwhile, the two r-l curves in Figs. 2(a)–2(c) tend toward the photon spheres as $l \to \infty$.

The ISCO and OSCO can be obtained by solving the equations $V_r = 0$ and $V_{rr} = 0$. This is actually the usual definition of the stable circular orbits in literature [46–48]. The r-l curve in Fig. 1 is the solution of $V_r = 0$. We denote the parameter of the upper branch of the curve as σ and consider V as a function of r and l. Since each r uniquely corresponds to a point on the curve, we can state that σ varies monotonically with r, which further implies that $\mathrm{d}r/\mathrm{d}\sigma \neq 0$. We have

$$0 = \frac{\mathrm{d}V_r(r(\sigma), l(\sigma))}{\mathrm{d}\sigma} = \frac{\partial V_r}{\partial r}\frac{\mathrm{d}r}{\mathrm{d}\sigma} + \frac{\partial V_r}{\partial l}\frac{\mathrm{d}l}{\mathrm{d}\sigma} = V_{rr}\frac{\mathrm{d}r}{\mathrm{d}\sigma} + \frac{\partial V_r}{\partial l}\frac{\mathrm{d}l}{\mathrm{d}\sigma} \tag{2.5}$$

on the curve. Thus,

$$V_{rr} = -\frac{\partial V_r}{\partial l}\frac{\mathrm{d}l}{\mathrm{d}r} = 0, \tag{2.6}$$

where we have used $\mathrm{d}l/\mathrm{d}r = 0$ at points A and B. Therefore, the turning points A and B in Fig. 1 are satisfied by $V_r = V_{rr} = 0$, which means they are actually the ISCO and OSCO.

The boundary of the range of parameters in which the ISCO and OSCO exist is the critical case as in Fig. 2(b), where the ISCO and OSCO coincide. In this case, $V_{rrr} = 0$, and this condition is equivalent to $\mathrm{d}^2l/\mathrm{d}r^2 = 0$. The proof is as follows: At the point coincided by A and B, $V_{rr} = 0$ and $\mathrm{d}l/\mathrm{d}r = 0$. If we choose $\mathrm{d}r/\mathrm{d}\sigma$ to be positive and finite, then

$$\frac{\mathrm{d}l}{\mathrm{d}\sigma} = \frac{\mathrm{d}l}{\mathrm{d}r}\frac{\mathrm{d}r}{\mathrm{d}\sigma} = 0. \tag{2.7}$$

From

$$0 = \frac{\mathrm{d}^2V_r}{\mathrm{d}\sigma^2} = V_{rrr}\left(\frac{\mathrm{d}r}{\mathrm{d}\sigma}\right)^2 + 2\frac{\partial V_{rr}}{\partial l}\frac{\mathrm{d}l}{\mathrm{d}\sigma}\frac{\mathrm{d}r}{\mathrm{d}\sigma} + \frac{\partial V_r}{\partial l}\frac{\mathrm{d}^2l}{\mathrm{d}\sigma^2} + \frac{\partial^2 V_r}{\partial l^2}\left(\frac{\mathrm{d}l}{\mathrm{d}\sigma}\right)^2 + V_{rr}\frac{\mathrm{d}^2r}{\mathrm{d}\sigma^2}, \tag{2.8}$$

we get

$$V_{rrr} = -2\frac{\partial V_{rr}}{\partial l}\frac{\mathrm{d}l}{\mathrm{d}r} - \frac{\partial V_r}{\partial l}\frac{\mathrm{d}^2l}{\mathrm{d}\sigma^2}\left(\frac{\mathrm{d}r}{\mathrm{d}\sigma}\right)^{-2} - \frac{\partial^2 V_r}{\partial l^2}\left(\frac{\mathrm{d}l}{\mathrm{d}r}\right)^2 - V_{rr}\frac{\mathrm{d}^2r}{\mathrm{d}\sigma^2}\left(\frac{\mathrm{d}r}{\mathrm{d}\sigma}\right)^{-2} = -\frac{\partial V_r}{\partial l}\frac{\mathrm{d}^2l}{\mathrm{d}\sigma^2}\left(\frac{\mathrm{d}r}{\mathrm{d}\sigma}\right)^{-2}, \tag{2.9}$$

where we have used $\mathrm{d}l/\mathrm{d}r = 0$ and $V_{rr} = 0$ for the ISCO and OSCO, and $V_r = 0$ for the entire curve in Fig. 2(b). Hence, when $V_{rrr} = 0$ and $\partial V_r/\partial l \neq 0$, we have $\mathrm{d}^2l/\mathrm{d}\sigma^2 = 0$. And then

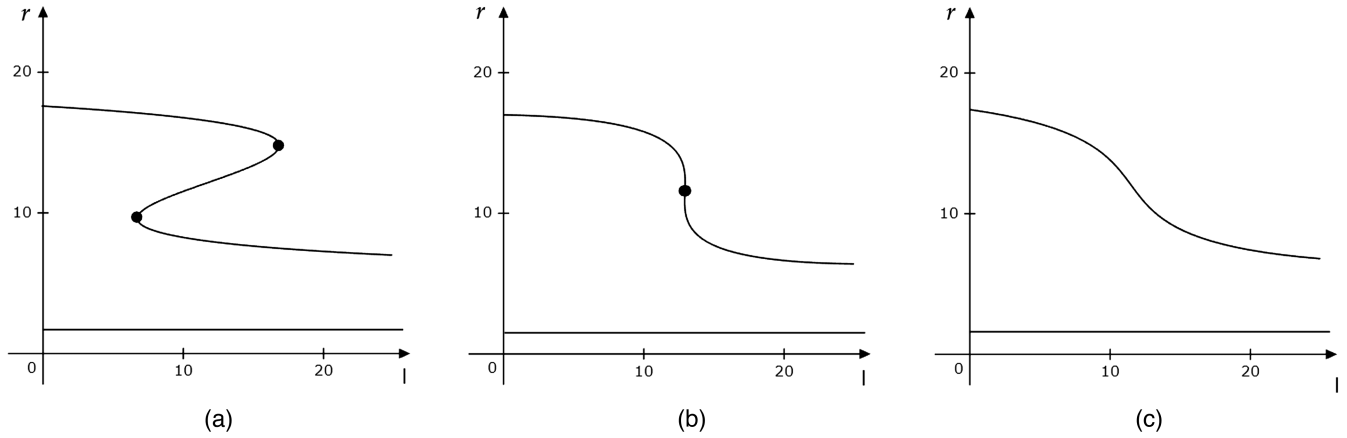

FIG. 2. Some possible r-l diagrams. The RN-dS black hole has an ISCO and an OSCO in diagram (a). The ISCO and OSCO coincide in diagram (b). There is no ISCO or OSCO in diagram (c).

$$\frac{\mathrm{d}^2 l}{\mathrm{d}r^2} = \frac{\mathrm{d}^2 l}{\mathrm{d}\sigma^2}\left(\frac{\mathrm{d}r}{\mathrm{d}\sigma}\right)^{-2} - \frac{\mathrm{d}l}{\mathrm{d}\sigma}\left(\frac{\mathrm{d}r}{\mathrm{d}\sigma}\right)^{-3}\frac{\mathrm{d}^2 r}{\mathrm{d}\sigma^2} = 0. \tag{2.10}$$

Therefore, when $V_{rrr} = V_{rr} = 0$ and $\mathrm{d}l/\mathrm{d}r = 0$, we have $\mathrm{d}^2 l/\mathrm{d}r^2 = 0$. To summarize, the orbit radii of the ISCO and OSCO are satisfied by $V_r = V_{rr} = 0$. And the critical case where the ISCO and OSCO coincide, which is also the critical case in which there is no ISCO or OSCO, is satisfied by $V_r = V_{rr} = V_{rrr} = 0$.

If there is no photon sphere—i.e., the spacetime is the RN-dS naked singularity—the r-l diagrams will be different, as shown in Fig. 3.

In order to see the various scenarios clearly, the relation of the existence of the ISCO and OSCO and Q is shown in Fig. 4. As we can see, the unstable photon sphere is always outside the event horizon. The dependence on the charge Q is given as follows:

(i) For $Q \in (0, Q_2)$, there are three horizons and two photon spheres. There is no ISCO or OSCO for $Q \in (0, Q_1)$, as in Fig. 2(c), and there is an ISCO and an OSCO for $Q \in (Q_1, Q_2)$, as in Fig. 2(a). When $Q = Q_1$, the ISCO and OSCO coincide, as in Fig. 2(b).

(ii) For $Q \in (Q_2, Q_3)$, it is a RN-dS naked singularity with two photon spheres, and there is an ISCO and an OSCO as in Fig. 2(a), too.

(iii) For $Q \in (Q_3, Q_4)$, the RN-dS naked singularity has no photon sphere, and the blue curve has three turning points. Stable circular orbits exist for two distinct intervals of r in this case, as in Fig. 3(a).

(iv) When $Q \geq Q_4$, there is an ISCO and an OSCO, and the corresponding r-l diagrams are Fig. 3(b) for $Q = Q_4$ and Fig. 3(c) for $Q > Q_4$.

The stable Cauchy horizon emerges when $\kappa_- < \kappa_c$ [25,26], where κ_- and κ_c are the surface gravities of the Cauchy horizon and the cosmological horizon, respectively. Once a stable Cauchy horizon exists, the SCCC will be broken down, and the predictability of classical theory is threatened. Thus, it has aroused great interest in the community

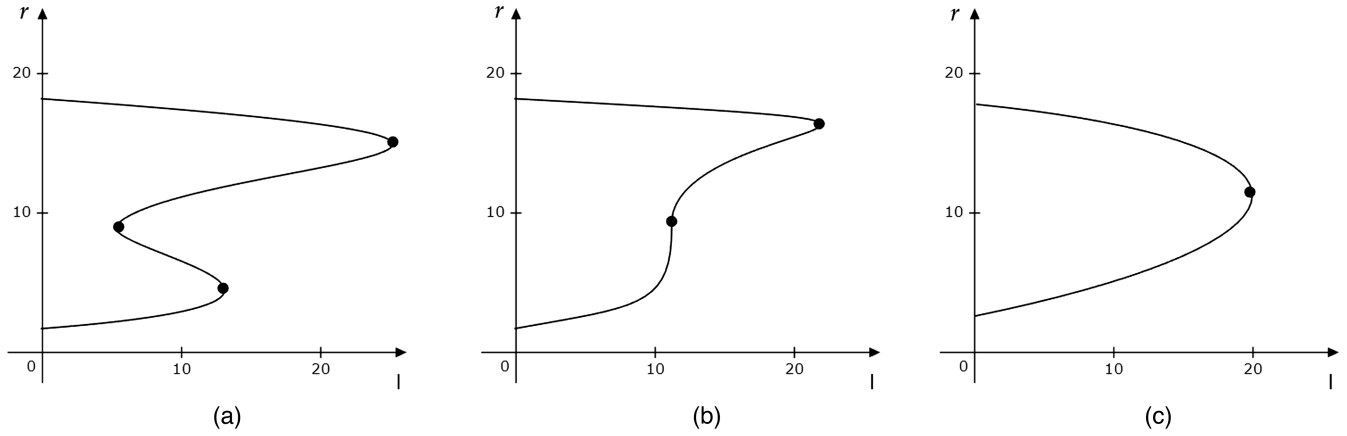

FIG. 3. Some possible r-l diagrams without a photon sphere. The spacetime has two ISCOs and two OSCOs (the three turning points and an ISCO with $l = 0$) in diagram (a). An ISCO and an OSCO coincide in diagram (b), and there is an ISCO ($l = 0$) and an OSCO (the turning point) in this case. There is an ISCO ($l = 0$) and an OSCO (the turning point) in diagram (c).

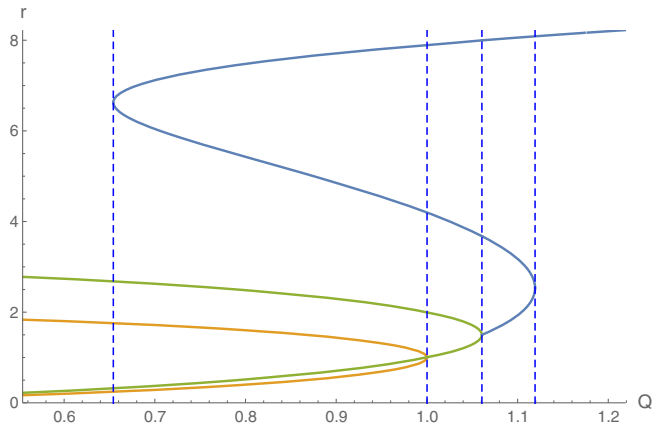

FIG. 4. The blue curve is the solution of $V_r = V_{rr} = 0$—i.e., the ISCO or OSCO. The orange curve is the Cauchy horizon and the event horizon. (The radius of the cosmological horizon is too large to be shown in the figure, so we omit it.) The green curve corresponds to the photon spheres. The parameter of the RN-dS spacetime is $\Lambda = 0.001$. The four blue dashed lines passing through the turning points are located at $Q_1 = 0.654242$, $Q_2 = 1.00017$, $Q_3 = 1.06066$, and $Q_4 = 1.11927$.

of general relativity and gravity theory. We will look for the range of the parameters of a black hole that has a stable Cauchy horizon as well as stable circular orbits (i.e., ISCO and OSCO). First, the range of the parameters for a black hole with three horizons has been drawn in Fig. 5(a). A part of the boundary of this range is given by $r_+ = r_-$ and $r_+ = r_c$. The parameter range for Kerr-dS black holes can be found in [56]. Although their graph closely resembles ours, it is important to note that their abscissa represents the angular momentum parameter α, while our abscissa corresponds to the charge parameter Q. This observation highlights the similarity between angular momentum and charge, illustrating that the RN-dS black hole can serve as a valuable reference for further study on Kerr-dS black holes. Second, the range of the parameters of a RN-dS black hole with a stable Cauchy horizon is shown as the small crescent in Fig. 5(b). The left boundary of this area is $\kappa_- = \kappa_c$, and the right boundary is $\kappa_- = 0$; i.e., $r_- = r_+$.

Finally, the range of parameters for the presence of stable circular orbits—i.e., an ISCO and OSCO—has been found from the definition, with the result shown in Fig. 6. In summary, the final range is the gray area in the right diagram of Fig. 6.

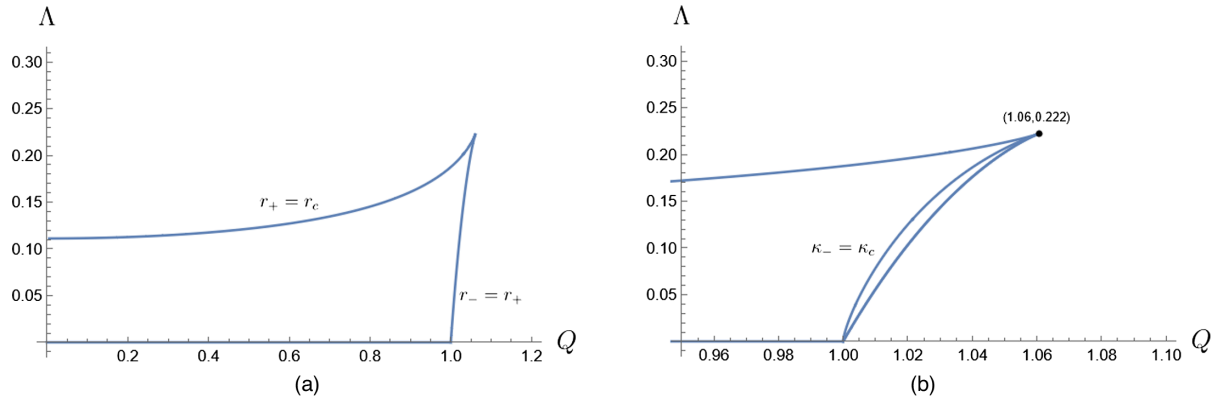

FIG. 5. (a) The range of the parameters of a RN-dS black hole with three horizons. The boundaries of the range are $r_- = r_+$ and $r_+ = r_c$. (b) The range of the parameters of a RN-dS black hole with $\kappa_- < \kappa_c$. The boundaries are $\kappa_- = \kappa_c$ and $\kappa_- = 0$.

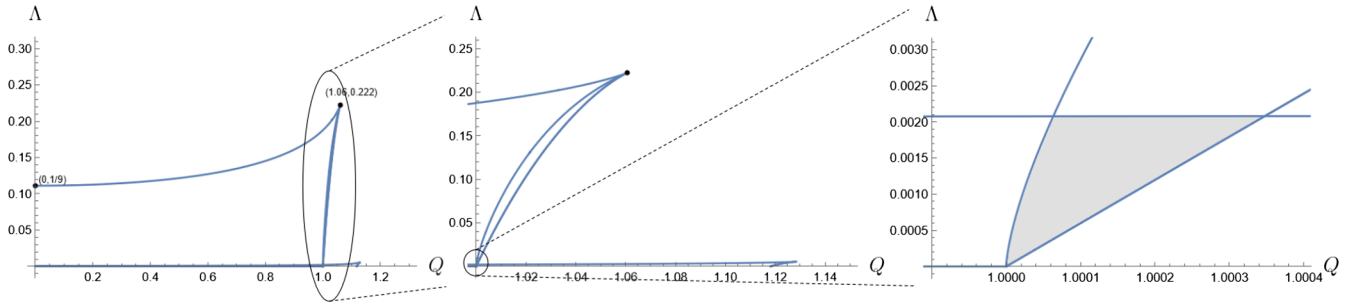

FIG. 6. The left diagram shows the boundaries of the range in which there are three horizons, one of which is a stable Cauchy horizon, and an ISCO and OSCO. The middle and right diagrams each display an enlarged portion of the diagram to their left. The range of interest is marked as a gray area in the rightmost diagram.

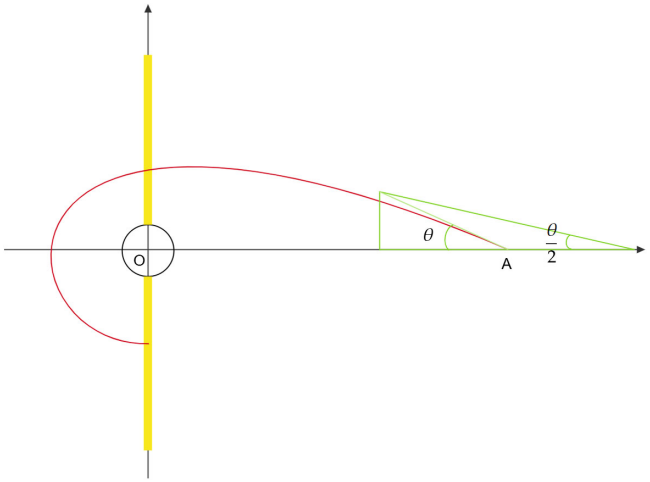

FIG. 7. Schematic picture showing the trajectory of the photons and the stereographic projection. The black hole is located at O, and the observer is at A. The black ring is the event horizon of the black hole. The yellow line represents the accretion disk, and the red curve is the ray from the accretion disk to the observer. θ is the angle of incidence. The green triangle is a schematic diagram of the stereographic projection.

III. THE APPEARANCE OF THE SCHWARZSCHILD-DS BLACK HOLE VIEWED BY OBSERVERS WITH DIFFERENT DISTANCES

In this section, we will study the effect of the position of the observer on the image of the Schwarzschild-dS black hole. The positions of the black hole, accretion disk, and observer and the trajectory of the photons are shown in Fig. 7. We use a stereographic projection to get the image, and thus the abscissa of the image y_{p} [58] is

$$y_{\mathrm{p}} = 2\tan\frac{\theta}{2} = 2\left(\frac{1}{\sqrt{f}}\frac{r}{b} - \sqrt{\frac{r^2}{fb^2} - 1}\right)\Bigg|_{r=r_{\mathrm{obs}}}, \tag{3.1}$$

where $b = l/E$ is the impact parameter, and r_{obs} can be understood as the distance between the observer and the black hole.

We use the ray-tracing method [36] to draw the images of black holes. The normalized number of orbits $n = \phi/(2\pi)$ relates to the number of intersections with the equatorial plane of a particular light ray, where ϕ is the azimuthal angle. Light bends greatly around the massive object, sometimes even tracing a circular path at the peak of the effective potential. This circular path is also known as the photon sphere or "critical curve." At the critical impact parameter, the number of rotations of the photons increases infinitely. This results in a bright ring in the image, and the size of the ring only depends on the background geometry of spacetime. Images produced by rays intersecting the accretion disk once, twice, or more than twice are referred to as the "direct emission," "lensed ring," and "photon ring," respectively. However, in most cases, the photon ring is so close to the lensed ring that it cannot be distinguished, and its contribution to the overall intensity is negligible. It means we can see only one bright ring in the image. At each intersection, newly emitted photons from the accretion disk join in the journey toward the screen or the celestial sphere of the observer. Each of the intersections of light with the accretion disk contributes to the intensity received by the observer. Besides this, considering the effect of gravitational redshift on the intensity of the emission, the intensity of the light received by the observer, I_{obs}, is [36,38,59]

$$I_{\mathrm{obs}} = \sum_n I_{\mathrm{em}}(r)\frac{f^2(r)}{f^2(r_{\mathrm{obs}})}\Bigg|_{r=r_n}, \tag{3.2}$$

where r_n is the position of the nth intersection with the accretion disk.

A phenomenon of discontinuity arises when the location of the observer is finite, and the intensity received by the observer "jumps" to null at certain impact parameters. In order to see the "jump" of the I_{obs} caused by the position of the observer, we choose a Schwarzschild-dS black hole with $\Lambda = 0.001M^{-2}$, which has no ISCO or OSCO. The luminous intensity of the accretion disk is

$$I_{\mathrm{em}}(r) = \begin{cases} \frac{\pi/2-\arctan(r-2)}{\pi/2-\arctan(r_+-2)}, & \text{if } r_+ < r < r_c. \\ 0, & \text{if } r \le r_+ \quad \text{or} \quad r \ge r_{\mathrm{c}}. \end{cases} \tag{3.3}$$

This kind of jump is different from the jump caused by the OSCO, which will be discussed later. The images viewed by observers at different distances are given in Fig. 8.

As we can see, there is a significant discontinuous jump in I_{obs}, as well as an edge in the image, when the observer is near the black hole. This is because some rays with large b cannot be received by an observer located too close to the black hole. To explain this better, we draw the trajectories of photons in Fig. 9. The rays with large b, like the blue curve, cannot be received by the observer, because its perihelion is farther from the black hole than the position of the observer. Therefore, there is a jump in the observed intensity, and the image of the black hole has a significant edge if the observer is close enough to the black hole. In order to avoid this kind of jump, the observer has to be located far away from the black hole. In this case, only light rays with a significantly large value of b cannot be received by the observer. Such light can only be emitted from the remote regions of the accretion disk. Consequently, its contribution to the total intensity is negligible.

We also find that an observer at $0.9r_{\mathrm{c}}$ receives a much stronger intensity I_{obs} than those at other locations in Fig. 8, since they have different redshift factors. As shown in Fig. 10, although two rays are emitted at the same position and have same $f(r_{\mathrm{em}})$ and $I_{\mathrm{em}}(r_{\mathrm{em}})$, they can have different values of $f(r_{\mathrm{obs}})$. The two observers in the example are located at A and B with $f_{\mathrm{Aobs}} = 0.633$ and $f_{\mathrm{Bobs}} = 0.190$,

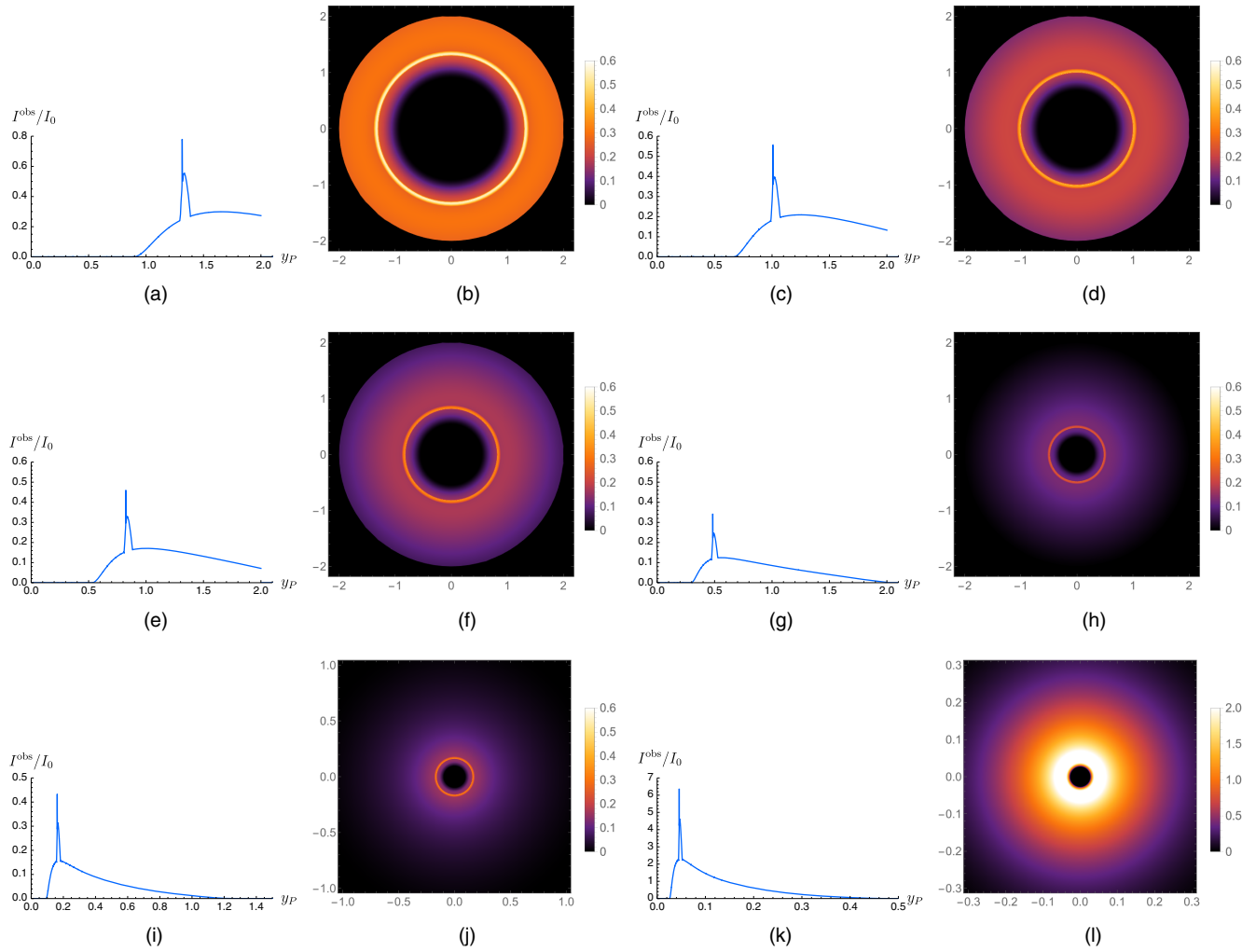

FIG. 8. The appearance of the Schwarzschild-dS black hole with $\Lambda = 0.001$ viewed by observers at different distances. The observed intensity $I_{\rm obs}$ is normalized to the maximum value I_0 of the emitted intensity. We choose six different observation positions: $r_{\rm obs} = 4$, 5, 6, 10, $0.5r_{\rm c}$, and $0.9r_{\rm c}$. For each given observation position, we draw the corresponding observed intensity and shadow image separately. Each item corresponds to an observer located at a specific position in a sequential manner: (a) intensity and (b) image for an observer at $r_{\rm obs} = 4$; (c) intensity and (d) image for an observer at $r_{\rm obs} = 5$; and so on, for observers at (e),(f) $r_{\rm obs} = 6$; (g),(h) $r_{\rm obs} = 10$; (i),(j) $r_{\rm obs} = 0.5r_{\rm c}$; and (k),(l) $r_{\rm obs} = 0.9r_{\rm c}$.

while $f_{\rm em}(r_{\rm em}) = 0.743$. Therefore, from Eq. (3.2), the observed intensity $I_{\rm obs}$ for A and B varies by a factor of $f^2_{\rm Aobs}/f^2_{\rm Bobs} \approx 11$. In conclusion, for observers located near the cosmological horizon, the intensity they receive will become brighter as they get closer to the cosmological horizon. In fact, this intensity can reach infinity. As the observer moves away from the black hole, the metric function $f(r_{\rm obs})$ increases and then decreases. Due to the same reason, the intensity (3.2) is large at small $r_{\rm obs}$ and near the cosmological horizon, while it diminishes a lot in the middle of these two horizons.

The image viewed by an observer far away from a Schwarzschild-dS black hole without an ISCO or OSCO has a similar shape to that of the usual Schwarzschild black hole. So, we draw up the image of the Schwarzschild-dS black hole with an ISCO and OSCO with $\Lambda = 0.0005$ in Fig. 11. In this case, the accretion disk is distributed between the ISCO and OSCO, and the luminous intensity of the accretion disk is

$$I_{\rm em}(r) = \begin{cases} \frac{1}{(r-r_{\rm ISCO}+1)^2}, & \text{if } r_{\rm ISCO} \le r \le r_{\rm OSCO} \\ 0, & \text{if } r < r_{\rm ISCO} \quad \text{or} \quad r > r_{\rm OSCO} \end{cases}. \tag{3.4}$$

To avoid an undesirable discontinuity due to the position of the observer, we set the observers as far away as possible. Actually, in the following discussion, $r_{\rm obs} = 0.9r_{\rm c}$ can reach the requirement.

As in Fig. 8, the image of the Schwarzschild-dS black hole with an ISCO and OSCO in Fig. 11 also has a edge. Particularly, when the observer is too close to the black hole

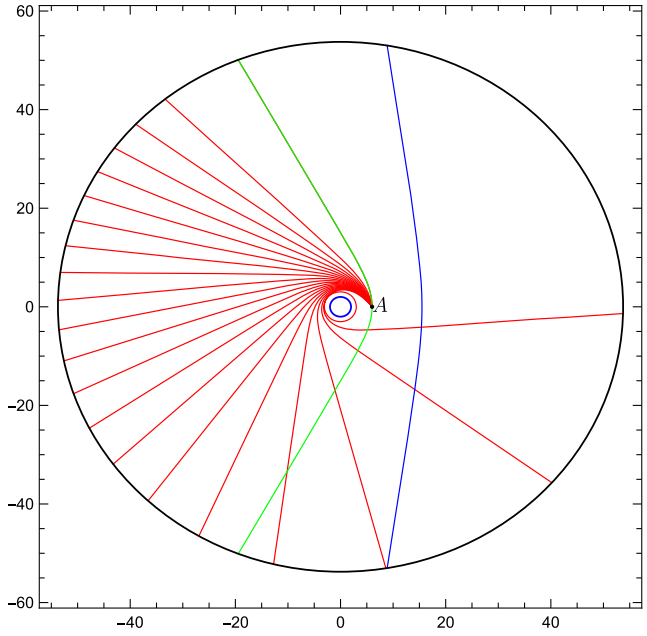

FIG. 9. The trajectories of photons. The parameter of the black hole is $\Lambda = 0.001$. The blue ring is the event horizon, and the black ring is the cosmological horizon. The observer is located at A. The rays with small b are received by the observer and are shown as red curves. But some rays with large b, whose radius of the perihelion is larger than $r_{\rm obs}$, cannot pass through the observer. An example of this kind of ray is shown as a blue curve. The critical case, when the perihelion of the ray is the position of the observer, is shown as the green curve.

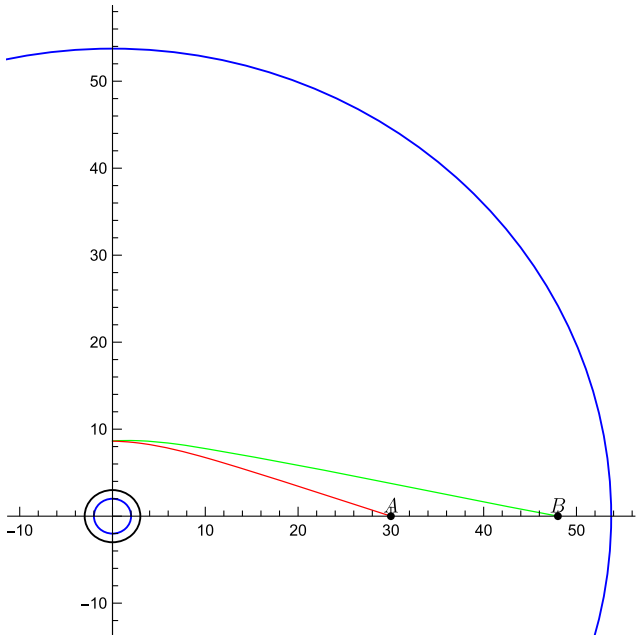

FIG. 10. Two trajectories of rays from the accretion disk to the observers A at $r_A = 30$ and B at $r_B = 48$. The three rings are the Cauchy horizon, event horizon, and cosmological horizon of the Schwarzschild-dS black hole with $\Lambda = 0.001$.

(e.g., $r_{\rm obs} = 4$), only the rays emitted from a little part of the accretion disk can be received by the observer. In this case, despite being a direct emission, the image contracts to a ring. However, the edges of the Schwarzschild-dS black hole with and without an ISCO and OSCO have different causes. Besides the influence of the observer's distance, the edge in the image of a black hole with an ISCO and OSCO is also a result of the fact that there is no light source outside the OSCO—i.e., the light source has a cutoff at the OSCO. Therefore, the image of the black hole with the cosmological constant will be a little bit different from that of the usual asymptotically flat Schwarzschild black hole. The presence of the cosmological constant may lead to the emergence of an OSCO, and this will produce an edge in the image of the black hole.

IV. THE APPEARANCE OF THE RN-DS BLACK HOLE

The position of the observer will affect the image of the black hole—in particular, a ray with large b will not be received by the observer. Therefore, we set the observer far from the black hole and near the cosmological horizon in this section—i.e., $r_{\rm obs} = 0.9 r_{\rm c}$. A part of the Penrose diagram of the RN-dS black hole is given by Fig. 12. If the Cauchy horizon is stable, the infinite repetition of the spacetime allows the ray emitted from the accretion disk in the previous universe A to fall into the black hole, fly out from the white hole, and finally be received by the observer in universe B. This kind of photon trajectory is shown as a red curve in Fig. 12. Besides this, the photons can both be emitted from the accretion disk and be received by the observer in universe B, shown as a green curve in Fig. 12. The images caused by these two kinds of ray are quite different. This can be found in the following discussions.

A. The appearance of the RN-dS black hole with an ISCO and OSCO

The appearance of a RN-dS black hole with $Q = 1.0001$, $\Lambda = 0.001$ is given by Fig. 13 with the observer located at $r_{\rm obs} = 48.378$ (with $r_{\rm obs}/r_{\rm c} = 0.9$). The light source distributes between the ISCO and OSCO, and the luminous intensity of the accretion disk is described by Eq. (3.4).

Compared to that of the Schwarzschild black hole, the image of the RN-dS black hole has a significant edge. This is because there is no light source outside the OSCO. This has already been encountered in the Schwarzschild-dS black hole with an ISCO and OSCO. Besides this, the lensed ring or the photon ring of the RN-dS black hole is smaller than that of the Schwarzschild black hole, although their photon spheres are the same size. The intensity of the Schwarzschild black hole is weaker than that of the RN-dS black hole, which is caused by the redshift factor. More precisely, when the observer is located far from the black hole, the metric function $f_{\rm Sch}(r_{\rm obs})$ tends to 1, while

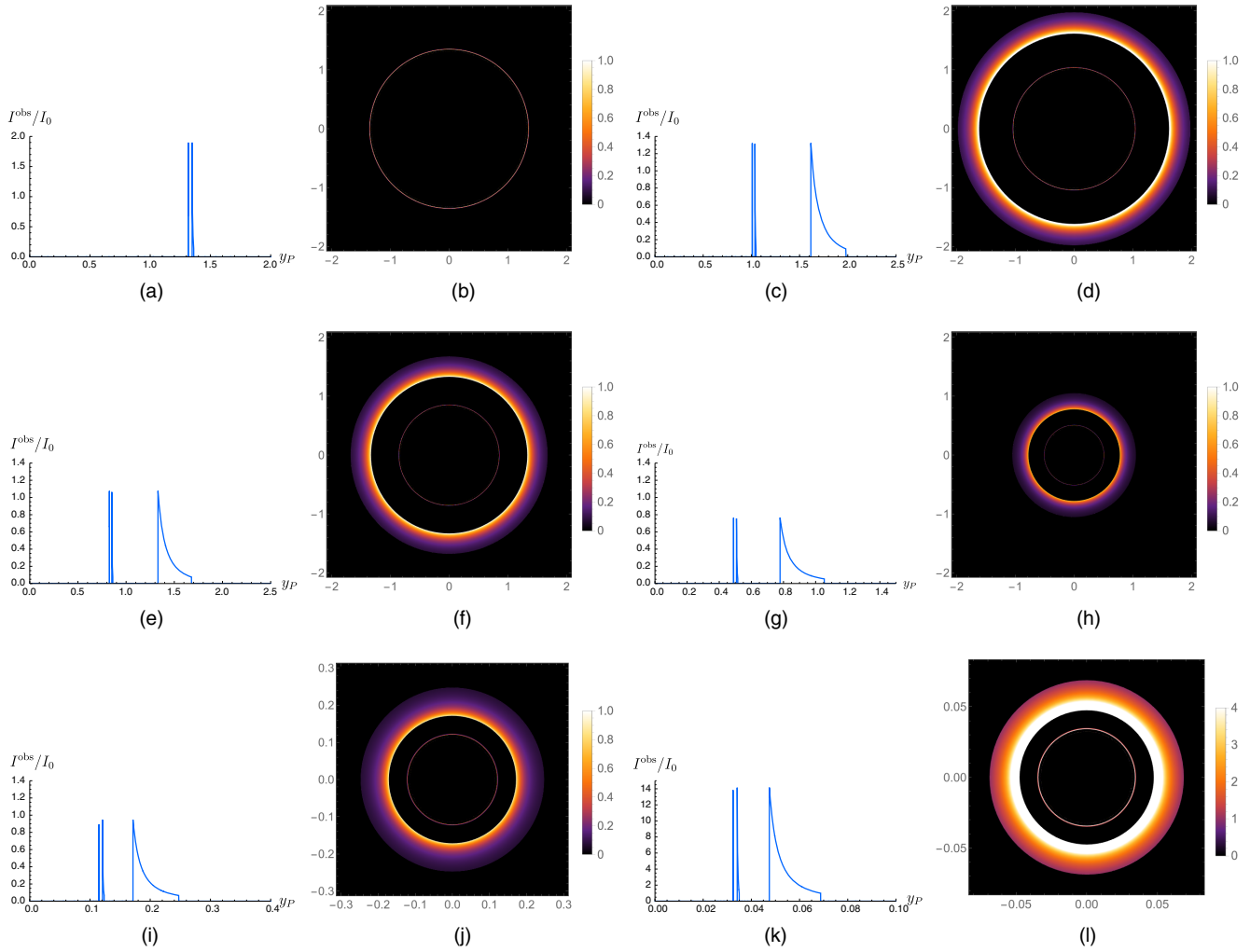

FIG. 11. The appearance of the Schwarzschild-dS black hole with $\Lambda = 0.0005$ viewed by observers at different distances. It has an ISCO and an OSCO. As with the Schwarzschild-dS black hole in Fig. 8 without an ISCO or OSCO, we choose six different observation positions: $r_{\rm obs} = 4, 5, 6, 10, 0.5r_{\rm c}$, and $0.9r_{\rm c}$. The diagrams show (a) intensity and (b) image for an observer at $r_{\rm obs} = 4$; (c) intensity and (d) image for an observer at $r_{\rm obs} = 5$; and so on, for observers at (e),(f) $r_{\rm obs} = 6$; (g),(h) $r_{\rm obs} = 10$; (i),(j) $r_{\rm obs} = 0.5r_{\rm c}$; and (k),(l) $r_{\rm obs} = 0.9r_{\rm c}$.

$f_{\rm RNdS}(r_{\rm obs})$ tends to 0. The cosmological constant chosen by us is $\Lambda = 0.001$. This means that the magnitude of ΛM^2 is 10^{-3}: in other words, it is a supermassive black hole, since the astronomical observations have revealed a tiny value for the cosmological constant. From Eq. (3.2), the intensity is greatly amplified when the observer is very close to the cosmological horizon because of the nearly divergent redshift factor. Therefore, if the observer is close enough to the cosmological horizon, the intensity emitted near the OSCO will be magnified so much that an edge can be seen clearly in the image. In short, the images of supermassive RN-dS black holes may have significant edges.

If the accretion disk is located in universe A, then the multiring structure occurs. The rings inside the photon ring are separated obviously, and we can distinguish them easily. The reasons for the formation of the multiring structure have been described in detail in [45]. The key is that the stable Cauchy horizon allows photons to cross it, and the infinitely repetitive spacetime allows photons to travel through different universes. As we had mentioned, this breaks the SCCC. In some special cases, if the accretion disks are located in both universes A and B, then the image is as shown in Fig. 13(h). Many rings occur inside the area which is traditionally thought to be the shadow, and the closer to the photon ring, the denser the rings become. It also has a significant edge. Therefore, if the SCCC is broken down, then this novel phenomenon may be observed. However, the multiring structure occurs not only when there is a stable Cauchy horizon, but also in the case of compact objects and wormholes [49–52]. In fact, when the effective potential $V(r)$ of the spacetime has a local maximum, the photon sphere (also called the critical curve) occurs, and there is a bright ring in the image. Furthermore, if there is an another higher maximum inside

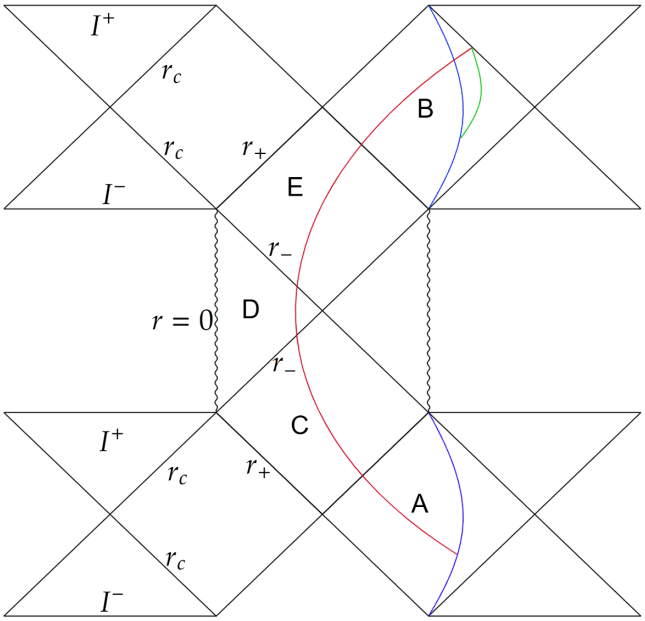

FIG. 12. The Penrose diagram of the RN-dS black hole. The blue curves are the accretion disks in universes A and B, respectively. The observer is located near the cosmological horizon. The green curve is the ray from the accretion disks in universe B and received by the observer, while the red curve is the ray from the accretion disks in universe A.

the outer one, or if V is diverging somewhere inside the photon sphere, then the multiring structure appears [51]. To distinguish between compact objects, wormholes, and the black hole with a stable Cauchy horizon, we require additional observation.

B. The appearance of the RN-dS black hole without an ISCO or OSCO

We have already discussed the situation of a RN-dS black hole with an ISCO and an OSCO. However, there are also RN-dS black holes that have no ISCO or OSCO. The accretion disk around these black holes will have no significant edge. In this subsection, we will study the image of these black holes. The luminous intensity of the accretion disk is given in (3.3). The image of a RN-dS black hole with $Q = 1.0002$, $\Lambda = 0.003$ is given by Fig. 14. The observer is located at $r_{\rm obs} = 27.530 = 0.9r_c$.

For a RN-dS black hole without ISCO and OSCO, the shape of the image is similar to that of the Schwarzschild one if the accretion disk is located in universe B. There is no outer edge in the image. However, for the case of an accretion disk located in universe A, or in both A and B, the multiring structure appears. Like the image in Fig. 13(h), there are many rings inside the shadow. And, similarly, the closer to the photon ring (or lensed ring), the denser the rings become. Compared to Figs. 13(f) and 13(h), the rings

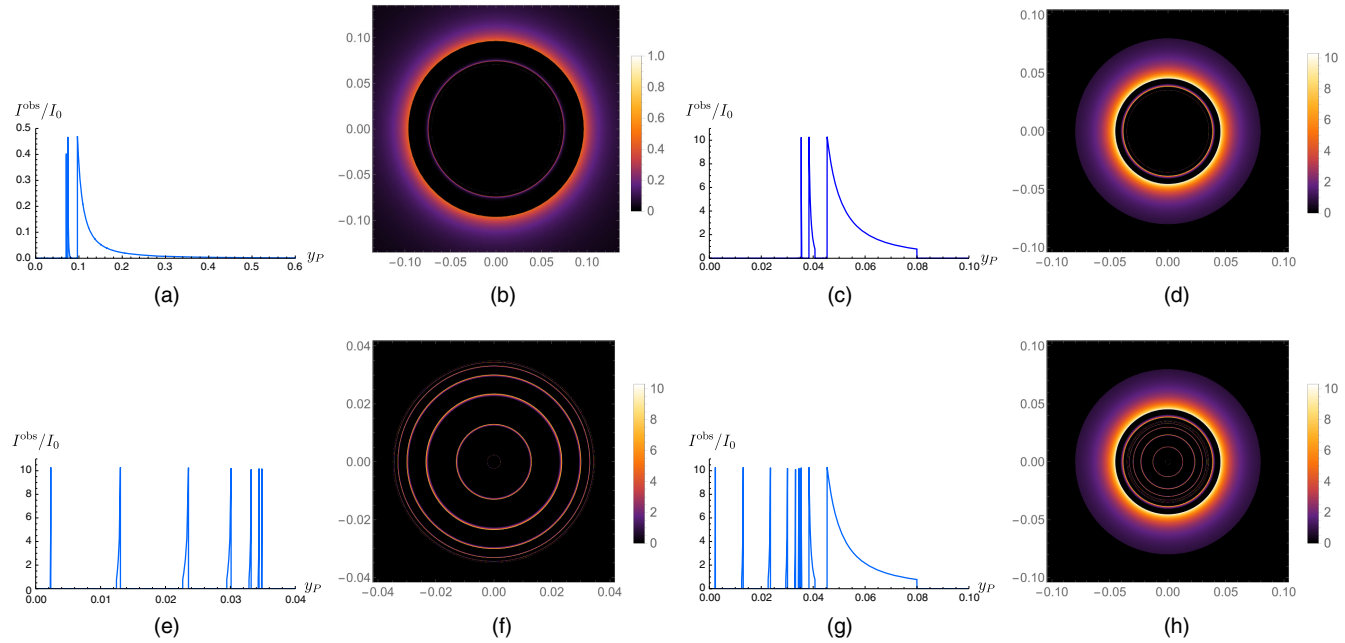

FIG. 13. The intensity and the image of a Schwarzschild black hole with the photon sphere at $r_{\rm sp} = 1.9996$ ($M = 0.6665$) and a RN-dS black hole with $Q = 1.0001$, $\Lambda = 0.001$. (a),(b) Observed intensity and image of the Schwarzschild black hole with a photon sphere whose radius is same as that of the RN-dS black hole. (c),(d) Observed intensity and image of the RN-dS black hole when the photons are emitted from the accretion disk in universe B. (e),(f) Observed intensity and image of the RN-dS black hole when the photons are emitted from the accretion disk in universe A. (g),(h) Observed intensity and image of the RN-dS black hole when the photons are emitted from the accretion disks in both universes A and B.

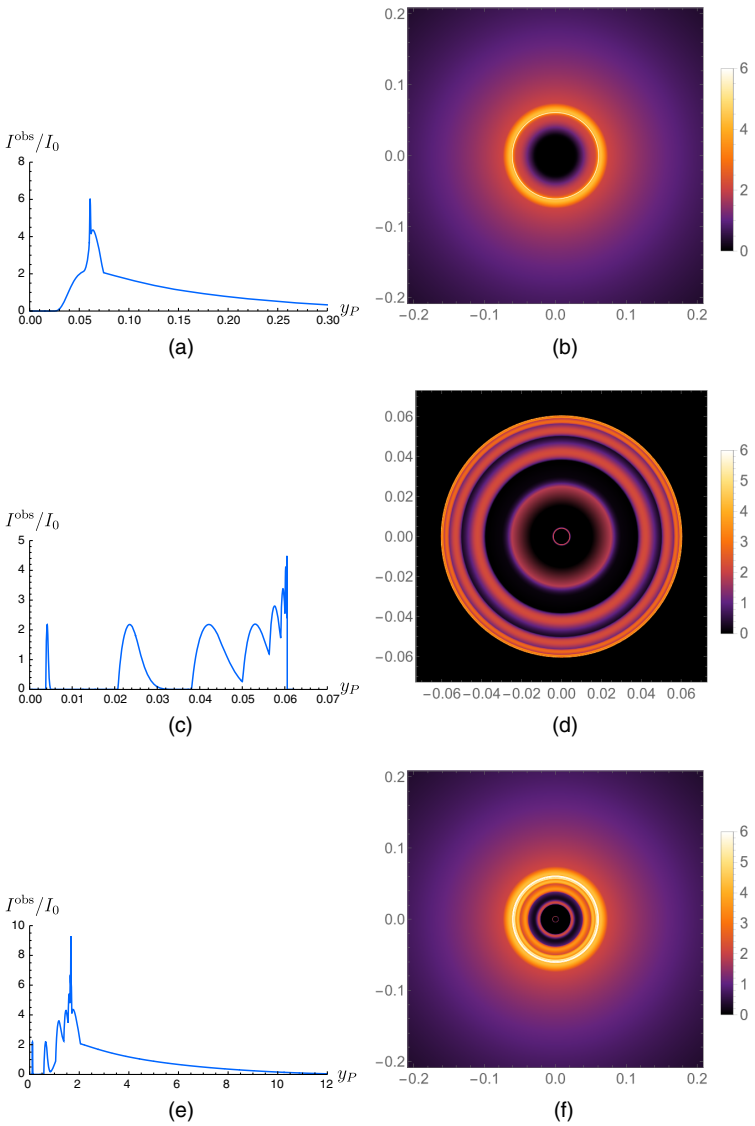

FIG. 14. The intensity and the image of a RN-dS black hole with $Q = 1.0002$, $\Lambda = 0.003$. (a),(b) Observed intensity and image of the RN-dS black hole when the photons are emitted from the accretion disk in universe B. (c),(d) Observed intensity and image of the RN-dS black hole when the photons are emitted from the accretion disk in universe A. (e),(f) Observed intensity and image of the RN-dS black hole when the photons are emitted from the accretion disks in both universes A and B.

in Figs. 14(d) and 14(f) are wider. Besides this, there is a little bit of overlap between some of the neighboring rings. Reference [51] also mentioned a similar phenomenon, where there are wider rings in the image if the edge of the accretion disk is closer to the center of the object. Here, to explain this phenomenon, the trajectories of rays have been drawn in Fig. 15.

The red, green, and blue solid rays in Fig. 15(a) are for the third peak (ring) with the normalized number $n = 7/4$ in Fig. 14(c). The red, green, and blue dashed rays in Fig. 15(b) are for the fourth peak with $n = 9/4$. If the accretion disk is between the ISCO and OSCO (black line), then the third ring is from b_2 to b_3, where b_i is the impact parameter of the ray with the corresponding number labeled in Fig. 15; the fourth ring is from b_5 to b_6. However, if the accretion disk is distributed outside the event horizon (black dashed line), then the third ring begins at b_1, and the fourth ring begins at b_4. Therefore, the rings caused by an accretion disk entirely outside the event horizon are wider than the rings caused by an accretion disk between the ISCO and OSCO. Taking the green dashed ray (labeled 5) for an example, it intersects with the lower part of the accretion disk in the figure twice and the upper part of the accretion disk in the figure twice. It contributes to the third ring and the fourth ring, too. Thus, all six rays intersect with the lower part of the accretion disk in the figure for $n = 7/4$, while only the red, green, and blue dashed rays intersect with the upper part of the accretion disk in the

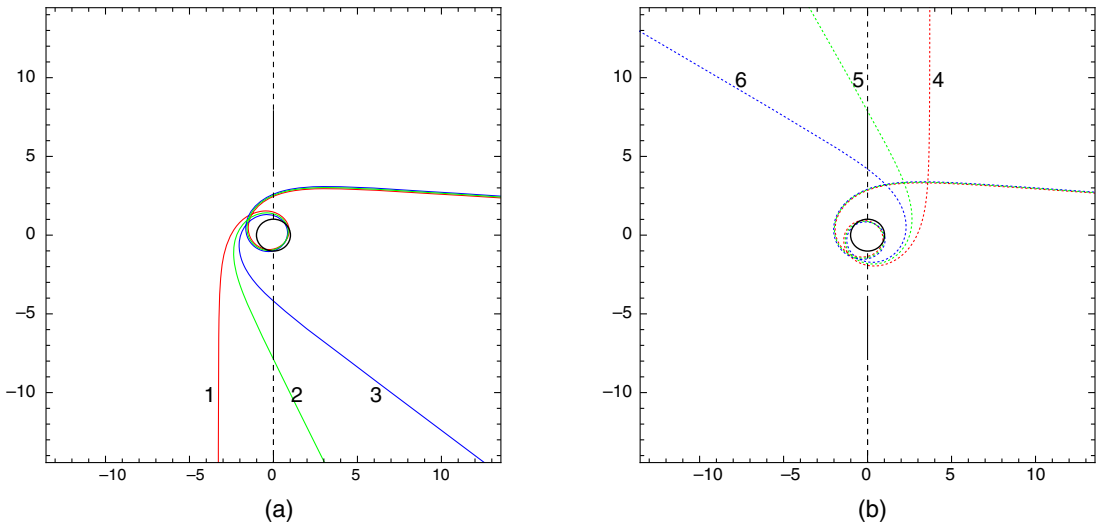

FIG. 15. The trajectories of rays around a RN-dS black hole. The black ring is the event horizon. The black line is the accretion disk between the ISCO and OSCO, and the dashed black line is the accretion disk between r_+ and r_c. The rays shown are (a) for $n = 7/4$ (the three solid rays labeled 1–3 and (b) for $n = 9/4$ (the three dashed rays labeled 4–6).

figure for $n = 9/4$. This means that the fourth ring begins when the third ring is not finished. Therefore, the third and the fourth rings in Fig. 14(c) have a little bit of overlap.

V. CONCLUSIONS AND DISCUSSION

The SCCC is an important subject in general relativity. It guarantees the predictability of the gravitation theory. However, although some potential observations violating the WCCC are proposed in the RN singularity [60], testing the SCCC from astronomical observations has been a challenge. Hence, it is significant to study the observational effects of the SCCC. The Cauchy horizon is the boundary of the region where the initial data can predict. When the Cauchy horizon is stable, one can pass it and arrive at a area that is not determined by the initial data, which violates the SCCC. The RN-dS black hole is one of the most famous black holes with a stable Cauchy horizon.

Unlike Schwarzschild black holes and RN black holes, there may exist an ISCO and an OSCO in a RN-dS black hole. The range of parameters when there is an ISCO and an OSCO in the RN-dS black hole with a stable Cauchy horizon is shown in Fig. 6. The accretion disk distributed between the ISCO and OSCO results in significant inner and outer edges in the image. Taking into account the positive cosmological constant, static observers only exist in the region inside the cosmological horizon. So, we have to place the observer between the event horizon and the cosmological horizon and use stereographic projection to obtain the image. To analyze the influence of the observer's distance on the image, we first draw up the image of a Schwarzschild-dS black hole without ISCO and OSCO viewed by observers at different distances.

When the observer is at a finite distance, the observed intensity is truncated, and the corresponding image is clearly bounded. This effect is particularly noticeable when the observer is close to the black hole, but it becomes progressively less distinguishable as the distance increases. This is because, for an observer at a finite distance, there is always light with an extremely large impact parameter that cannot be received. As the observer's distance increases, the intensity decreases and then increases, which results from that the denominator of the redshift factor in Eq. (3.2) being nearly zero when the observer is too close to the event horizon and the cosmological horizon. If the observer is far enough away from the black hole (e.g., $0.9r_c$), the edge may disappear. We also draw up the image of a Schwarzschild-dS black hole with an ISCO and an OSCO in Fig. 11. This image has an outer edge, too. However, the cause of this edge is different. Besides the influence of the observed distance, the OSCO would result in an outer edge in the image, too. The reason is that there is no light source outside the OSCO, and this edge always exists no matter how far away the observer is.

In order to avoid the influence of the observed distance, we draw up the image of a RN-dS black hole with an ISCO, an OSCO, and a stable Cauchy horizon viewed by a faraway observer in Fig. 13. The observer is located in universe B, while there are two kinds of light sources. When the photons are emitted from the accretion disk in universe B, the image's shape is similar to that of the Schwarzschild black hole, except that there is an outer edge in the image of RN-dS black hole, which results from the OSCO. Besides this, the photon ring of the RN-dS black hole is smaller than the Schwarzschild one, even though they have photon spheres of the same size. Also, the intensity of the image of RN-dS black hole is much larger

than the Schwarzschild one, due to the redshift factor. If the observer is close enough to the cosmological horizon, the redshift factor tends to infinity, and the edge of the image is bright enough to be viewed clearly. However, when the accretion disk is located in universe A, the photons can be received by the observer in universe B by the black-white hole channel. These photons produce many extra bright rings in the image. When the accretion disk is located in both universes A and B, the image has an outer edge, as well as the multiring structure inside the traditional shadow area. The image of the RN-dS black hole without an ISCO or OSCO is also shown in Fig. 14. The accretion disk is distributed between the event horizon and the cosmological horizon, and it is sharply peaked at the event horizon. The multiring structure also occurs when there is only one accretion disk in universe A. As a result, the widely distributed accretion disk leads to wider rings inside the shadow. Some of the neighboring rings even have a little overlap. In conclusion, the image of a RN-dS black hole with a stable Cauchy horizon is much different from the Schwarzschild one.

The RN-dS black hole with a stable Cauchy horizon is one of the simplest examples inconsistent with the SCCC. Based on our analysis, the biggest differences between its image and the Schwarzschild's are the outer edge and the multiring structure. Another example which violates the SCCC is a regular black hole with a stable Cauchy horizon. There is also a multiring structure in its image [45]. Therefore, if the SCCC is broken down, this multiring structure may be observed. This provides us a new way to test the SCCC in astronomical observation. It is worth noting that such a multiring structure can also appear in cases of compact objects and wormholes, which have no horizon, and we need other methods to distinguish them.

Within classical theory, some black holes have stable Cauchy horizons. However, certain studies suggest that in such scenarios, quantum effects will play an important role and eventually render these Cauchy horizons unstable [61–63]. Nevertheless, whether quantum effects will overturn established classical results remains an unresolved issue. Probing the multiring structure could help us to examine the SCCC and further assess the significance of quantum effects.

Our future research will focus on two intriguing directions: First, we aim to study the images of rotating black holes with stable Cauchy horizons and further explore the presence of multiring structures which are similar to those observed in RN-dS images. Second, we plan to investigate other types of black holes that violate the SCCC. The images of these more complex black holes may reveal new types of structures in black hole images beyond what is currently known. We hope that these investigations will provide new methods for testing the SCCC in astronomical observations.

ACKNOWLEDGMENTS

This work was supported in part by the National Natural Science Foundation of China with Grants No. 12075232 and No. 12247103. It is also supported by the National Key R&D Program of China with Grant No. 2022YFC2204603.

[1] R. Penrose, Phys. Rev. Lett. **14**, 57 (1965).
[2] S. W. Hawking and R. Penrose, Proc. R. Soc. A **314**, 529 (1970).
[3] R. Penrose, Riv. Nuovo Cimento **1**, 252 (1969).
[4] R. Penrose, Gravitational collapse, in *Gravitational Radiation and Gravitational Collapse*, edited by C. Dewitt-Morette, IAU Symposium Vol. 64 (Springer, New York, 1974), pp. 82–91.
[5] R. Wald, Ann. Phys. (N.Y.) **82**, 548 (1974).
[6] J. Sorce and R. M. Wald, Phys. Rev. D **96**, 104014 (2017).
[7] R. Penrose, Singularities of spacetime, in *Theoretical Principles in Astrophysics and Relativity*, edited by N. R. Lebovitz, W. H. Reid, and P. O. Vandervoort (University of Chicago Press, Chicago, 1978).
[8] R. Penrose, Singularities, and time-asymmetry, in *General Relativity, and Einstein Centenary Survey*, edited by S. W. Hawking and W. Israel (Cambridge University Press, London, 1979).
[9] M. Simpson and R. Penrose, Int. J. Theor. Phys. **7**, 183 (1973).
[10] John Mcnamara, Proc. R. Soc. A **358**, 499 (1977).
[11] John Michael McNamara, Proc. R. Soc. A **364**, 121 (1978).
[12] S. Chandrasekhar and J. B. Hartle, Proc. R. Soc. A **384**, 301 (1982).
[13] W. A. Hiscock, Phys. Lett. **83A**, 110 (1991).
[14] E. Poisson and W. Israel, Phys. Rev. D **41**, 1796 (1990).
[15] A. Ori, Phys. Rev. Lett. **67**, 789 (1991).
[16] L. M. Cao, L. Y. Li, L. B. Wu, and Y. S. Zhou, arXiv: 2308.10746.
[17] E. G. Brown, R. B. Mann, and L. Modesto, Phys. Rev. D **84**, 104041 (2011).
[18] M. Z. Iofa, J. Exp. Theor. Phys. **135**, 647 (2022).
[19] R. Carballo-Rubio, F. Di Filippo, S. Liberati, C. Pacilio, and M. Visser, J. High Energy Phys. 05 (2021) 132.
[20] P. R. Brady, D. Nunez, and S. Sinha, Phys. Rev. D **47**, 4239 (1993).
[21] F. Mellor and I. Moss, Phys. Rev. D **41**, 403 (1990).
[22] V. Cardoso, J. L. Costa, K. Destounis, P. Hintz, and A. Jansen, Phys. Rev. Lett. **120**, 031103 (2018).
[23] J. Costa, P. M. Girão, J. Natário, and J. D. Silva, J. Phys. Conf. Ser. **600**, 012031 (2015).

[24] J. L. Costa and A. T. Franzen, Ann. Henri Poincare **18**, 3371 (2017).
[25] P. R. Brady and E. Poisson, Classical Quantum Gravity **9**, 121 (1992).
[26] R. G. Cai and R. K. Su, Phys. Rev. D **52**, 666 (1995).
[27] J. L. Costa, P. M. Girão, J. Natário, and J. D. Silva, Classical Quantum Gravity **32**, 015017 (2015).
[28] J. L. Costa, P. M. Girão, J. Natário, and J. D. Silva, Commun. Math. Phys. **339**, 903 (2015).
[29] J. L. Costa, P. M. Girão, J. Natário, and J. D. Silva, Ann. PDE **3**, 8 (2017).
[30] F. Rossetti, arXiv:2309.14420.
[31] A. Ori, Phys. Rev. Lett. **68**, 2117 (1992).
[32] C. M. Chambers, Ann. Isr. Phys. Soc. **13**, 33 (1997), https://inspirehep.net/literature/448267.
[33] K. Akiyama *et al.* (Event Horizon Telescope Collaboration), Astrophys. J. Lett. **875**, L1 (2019).
[34] K. Akiyama *et al.* (Event Horizon Telescope Collaboration), Astrophys. J. Lett. **930**, L12 (2022).
[35] C. M. Claudel, K. S. Virbhadra, and G. F. R. Ellis, J. Math. Phys. (N.Y.) **42**, 818 (2001).
[36] S. E. Gralla, D. E. Holz, and R. M. Wald, Phys. Rev. D **100**, 024018 (2019).
[37] J. Peng, M. Guo, and X. H. Feng, Chin. Phys. C **45**, 085103 (2021).
[38] I. De Martino, R. Della Monica, and D. Rubiera-Garcia, Phys. Rev. D **108**, 124054 (2023).
[39] Z. L. Wang, Eur. Phys. J. Plus **138**, 1131 (2023).
[40] C. Zhang, Y. Ma, and J. Yang, Phys. Rev. D **108**, 104004 (2023).
[41] H. Huang, J. Kunz, J. Yang, and C. Zhang, Phys. Rev. D **107**, 104060 (2023).
[42] Z. Luo, H. Yu, and J. Li, arXiv:2312.07018.
[43] J. Peng, M. Guo, and X. H. Feng, Phys. Rev. D **104**, 124010 (2021).
[44] S. Guo, G. R. Li, and E. W. Liang, Eur. Phys. J. C **83**, 663 (2023).
[45] L. M. Cao, L. Y. Li, X. Y. Liu, and Y. S. Zhou, arXiv:2312.04301.
[46] T. Berry, A. Simpson, and M. Visser, Universe **7**, 2 (2020).
[47] P. Boonserm, T. Ngampitipan, A. Simpson, and M. Visser, Phys. Rev. D **101**, 024050 (2020).
[48] Y. Song, Eur. Phys. J. C **81**, 875 (2021).
[49] G. J. Olmo, D. Rubiera-Garcia, and D. S. C. Gómez, Phys. Lett. B **829**, 137045 (2022).
[50] M. Guerrero, G. J. Olmo, D. Rubiera-Garcia, and D. Sáez-Chillón Gómez, Phys. Rev. D **105**, 084057 (2022).
[51] M. Guerrero, G. J. Olmo, D. Rubiera-Garcia, and D. Sáez-Chillón Gómez, Phys. Rev. D **106**, 044070 (2022).
[52] G. J. Olmo, J. L. Rosa, D. Rubiera-Garcia, and D. Sáez-Chillón Gómez, Classical Quantum Gravity **40**, 174002 (2023).
[53] N. Tsukamoto, Phys. Rev. D **104**, 064022 (2021).
[54] N. Tsukamoto, Phys. Rev. D **105**, 084036 (2022).
[55] G. Morales-Herrera, P. Ortega-Ruiz, M. Momennia, and A. Herrera-Aguilar, arXiv:2401.07112.
[56] M. Momennia, A. Herrera-Aguilar, and U. Nucamendi, Phys. Rev. D **107**, 104041 (2023).
[57] Z. Stuchlík, M. Kološ, J. Kovář, P. Slaný, and A. Tursunov, Universe **6**, 26 (2020).
[58] A. Grenzebach, *The Shadow of Black Holes* (Springer International Publishing, Cham, 2016), pp. 55–79.
[59] G. B. Rybicki, *Radiative Processes in Astrophysics* (Wiley-VCH, New York, 2004), ISBN 978-0-471-82759-7, 978-3-527-61817-0.
[60] J. Wagner, arXiv:2301.13210.
[61] R. G. Cai, Phys. Rev. D **53**, 5698 (1996).
[62] R. G. Cai, Phys. Rev. D **59**, 104004 (1999).
[63] S. Hollands, R. M. Wald, and J. Zahn, Classical Quantum Gravity **37**, 115009 (2020).